JOURNAL OF MATERIALS SCIENCE 33 (1998) 1405–1419

Fatigue propagation behaviour of polystyrene/polyethylene blends

M. N. BUREAU*, J. I. DICKSON
Département de métallurgie et de génie des matériaux, École Polytechnique, C.P. 6079, Succ. Centre-ville, Montréal, Canada H3C 3A7

J. DENAULT
Institut des matériaux industriels, Conseil national de recherche Canada, 75 de Mortagne, Boucherville, Canada J4B 6Y4

Fatigue crack propagation (FCP) of injection-moulded polystyrene (PS) and 95/5, 85/15 and 70/30 PS/high-density polyethylene (HDPE) blends at loading frequencies of 2 and 20 Hz was studied. The FCP results showed that increasing the HDPE content caused a progressive reduction of the fatigue crack growth rates, especially when a styrene/ethylene–butylene/styrene (SEBS) terpolymer was added as a compatibilizer. Increasing the loading frequency also led to a fatigue crack growth rate reduction. Moreover, the fatigue crack growth rates were lower at a given cyclic stress intensity factor range, ΔK, when the crack propagated normal, instead of parallel, to the melt-flow direction during injection moulding. Fractographic observations indicated that discontinuous growth bands (DGBs), associated with the fracture of crazes in the plastic zone, were present through most or all of the fracture surfaces of the PS/HDPE specimens. In the presence of sufficient HDPE, these DGBs were formed by the initiation, growth and coalescence of large dimples initiated at HDPE particles ahead of the microscopic crack front, similar to a multiple crazing effect. The loading frequency effect on the FCP behaviour of these blends is attributed to a time-dependent deformation process. It is concluded that the FCP behaviour of these blends is strongly affected by the loading direction with respect to the matrix and minor phase orientation, by the presence of a compatibilizer, by the composition of the blend and by the testing conditions.

1. Introduction

A number of studies and reviews [1–14] on the fatigue behaviour of rubber-toughened blends have shown that the presence of rubber particles in a brittle thermoplastic matrix generally leads to a reduced resistance to fatigue crack initiation in unnotched specimens and to an improved resistance to fatigue crack propagation (FCP) in precracked specimens. However, the fatigue behaviour of blends of low glass transition temperature thermoplastics as the minor phase, and glassy thermoplastics as the matrix [15–23], has been little addressed. Our previous study [24] on FCP of 95/5 polystyrene/high-density polyethylene (PS/HDPE) blends showed an improved FCP resistance (i.e. a reduction of the fatigue crack growth rate at a given ΔK) caused by the presence of HDPE particles with or without the addition of a compatibilizer. Qualitatively, this behaviour was found to be similar to that of rubber-toughened blends.

Interpretations of the FCP behaviour have mostly been presented for homogeneous thermoplastic polymers [2, 9, 10, 13, 25–26]. These studies have shown the presence of discontinuous growth bands (DGBs) on the fracture surfaces at low and moderate fatigue crack growth rates associated with crazed material in the plastic zone [25–27]. The width of these DGBs compared to the average fatigue crack growth rate at which they formed indicated that a number of fatigue cycles are required to form and fracture each DGB. Similar DGBs were also reported for PS/HDPE blends [24]. At higher fatigue crack growth rates, fatigue striations have also been reported on the fracture surface of various homogeneous polymers, such as PS [24, 37], polycarbonate [35, 37], poly(methyl methacrylate) (PMMA) [37, 38] and polysulphone [37]. These striations are characterized by an interstriation spacing generally in agreement with the macroscopic fatigue crack growth rate [24, 31, 37], which suggests that a striation is formed during each stress cycle. Some results obtained for nylon-based blends [10, 39], poly(vinylidene fluoride) [39] and low-density polyethylene [40], however, have indicated that the striation spacing does not always agree with the

* Author to whom all correspondence should be addressed.
e:mail: martin.bureau@nrc.ca

macroscopic fatigue crack growth rate and can, at times, correspond to several times this rate [24]. Further observations on pure PS injection-moulded specimens [24] indicated that this lack of agreement was associated with FCP retardation effects in the skin of the specimens. However, in the 95/5 PS/HDPE blends tested, such fatigue striations were not observed and the formation of DGB-like features continued to higher fatigue crack growth rates [24].

Increasing the loading frequency has been found either to decrease or not to influence significantly the fatigue crack growth rate [25, 27, 28, 31, 41–49]. The variation of the fatigue crack growth rate with loading frequency has usually been attributed to an effect of hysteretic heating [32, 50] caused by energy dissipation during fatigue loading when a secondary viscoelastic transition (β-peak) is present. This hysteretic heating may lead, when confined to the plastic zone, to a localized temperature rise near the crack tip. With a significant increase in temperature, yielding near the crack tip should be enhanced, leading to an increase in crack-tip radius. It has been argued that the fatigue crack growth rate can be lowered [32] as a result of the blunted crack-tip region experiencing a lower effective ΔK. Following this argument, the fatigue crack growth rate could be lowered by increased blunting of the crack tip at higher loading frequencies, because the hysteretic heating rate is proportional to the loading frequency [50]. However, very few experimental observations of a significant temperature rise in the crack-tip region accompanying fatigue crack growth rate reduction with increasing loading frequency have been reported [9, 51]. Our previous study [24] did not permit us to conclude that such an effect of hysteretic heating was involved during FCP of PS-based materials.

The objective of the present work was to investigate further the FCP behaviour of pure PS and of PS/HDPE blends. The effect of a styrene/ethylene–butylene/styrene (SEBS) triblock copolymer, added as a compatibilizer in order to increase the PS/HDPE interface cohesion [16–20, 23, 24, 52–57], is also discussed.

2. Experimental procedure

2.1. Material preparation

The materials employed were a HDPE, HBL-455A ($\bar{M}_w = 171\,000$, $\bar{M}_w/\bar{M}_n = 20.3$, where $\bar{M}_w$ and $\bar{M}_n$ are, respectively, the weight average and the number average molecular weight), an atactic extrusion grade PS, GPPS103 ($\bar{M}_w = 270\,000$, $\bar{M}_w/\bar{M}_n = 2.0$) supplied by Novacor Chemistry (Canada) Ltd, and a SEBS triblock copolymer, Kraton G1652, as compatibilizer supplied by Shell Development Corp. The material and specimen preparation conditions have been previously described in detail [24]. Two groups of blends were obtained using a twin-screw extruder. The first contained no compatibilizer, and the second contained 10% SEBS compatiblizer by weight of the HDPE minor phase, added to this phase before the PS/(SEBS/HDPE) blending in order to optimize the compatibilization. The composition of the blends tested without SEBS was 95/5, 85/15 and 70/30 PS/HDPE, and the composition of the blends with SEBS was 95/(0.5/4.5), 85/(1.5/13.5) and 70/(3/27) PS/(SEBS/HDPE). The blends were injection-moulded into 5 mm thick plates, with the exception of the 30% minor phase blends, which were injection-moulded into 7 mm thick plates. Some of the results obtained on specimens of pure PS and of 95/5 PS/HDPE and 95/(0.5/4.5) PS/(SEBS/HDPE) blends have been previously reported [24].

2.2. Fatigue crack propagation testing

The FCP tests were performed at 23 °C and 50% relative humidity following the ASTM E-647 standard test method, employing a computer-controlled servo-hydraulic Instron tester, a sinusoidal waveform, a cycling frequency of 2 and 20 Hz and an R-ratio ($R = P_{min}/P_{max}$, where P_{min} and P_{max} are, respectively, the minimum and maximum applied loads) of 0.1. Compact tension (CT) specimens (Fig. 1) were employed, with a thickness, B, equal to that of the

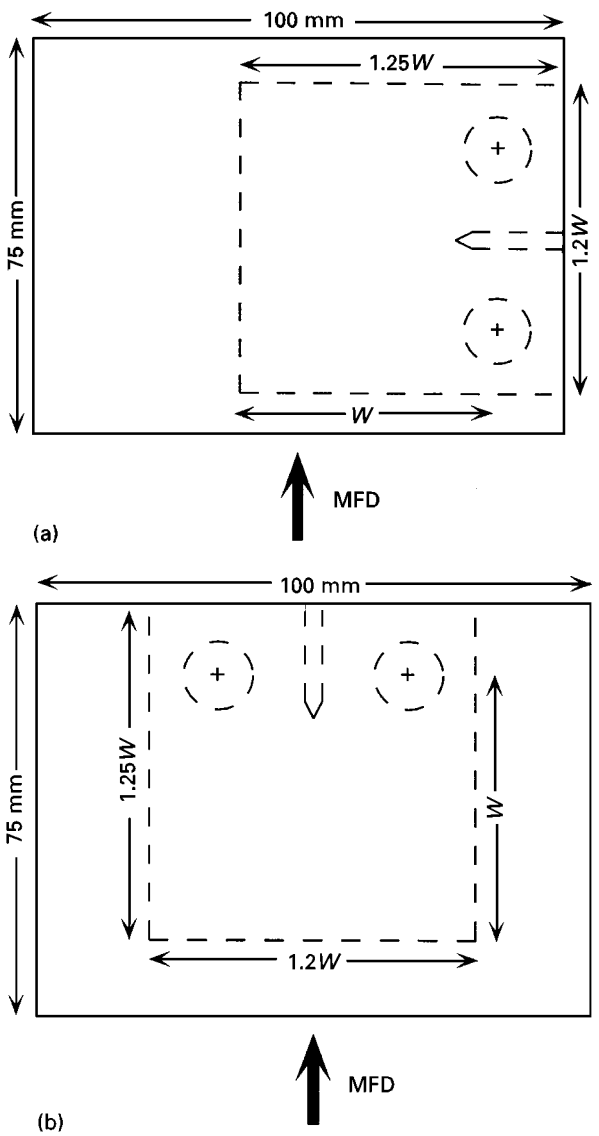

Figure 1 Diagrams of the CT specimens employed for the FCP tests showing their position and orientation in the injection-moulded plates as a function of the melt-flow direction (MFD): (a) for transverse specimens and (b) longitudinal specimens.

injection-moulded plates, a specimen width, W, of 50 mm, a notch depth of 9 mm and a notch opening width of 2.5 mm. A razor-blade cut was introduced manually at the notch tip just prior to the start of fatigue precracking. Every specimen tested was precracked over a distance of 3.5 mm at $R = 0.1$ at a loading frequency of 20 Hz following ASTM E-647. The specimens were loaded for propagation either normal (transverse specimens) or parallel (longitudinal specimens) to the melt-flow direction. A diagram of the position of these specimens in the injection-moulded plates is presented in Fig. 1. A detailed description of the FCP test procedure has been previously presented [24]. Similar tests were also performed on modified CT specimens, in which side grooves 0.45 mm deep and 0.90 mm high were machined along the expected crack plane in order to eliminate the effect of the oriented skin produced by the injection-moulding process.

2.3. Fractographic observations

The fatigue fracture surfaces were first coated with a thin layer of gold–palladium and then observed with a JEOL JSM-6100 scanning electron microscope (SEM). The size and shape of the fractographic features reported were evaluated, in most cases, by stereographic observations obtained using two photographs with a 6° difference in tilt angle. Computer-assisted image analysis was employed to evaluate the morphology of the HDPE particles on cryogenically fractured specimens.

3. Results and discussion

3.1. Morphological characterization of HDPE particles

The average minor phase diameter was measured, on scanning electron micrographs of cryogenic fracture surfaces, parallel and perpendicular to the melt-flow direction in the PS/HDPE blends. The average minor phase diameters of the 95/5, the 85/15 PS/HDPE blends with and without SEBS and the 70/30 PS/HDPE blend with SEBS are shown in Table I. Measurements were made in the two planes of observations (i.e. parallel and normal to the melt-flow direction) which corresponded to the FCP planes in the tests performed. The HDPE volume fraction, f_a, the average particle diameter, d_a, the average number of particles per unit volume, n_a, the average particle separation, L, the average interparticle distance, T, and the average particle separation to average particle diameter ratio, L/d, are calculated from the equations presented in the Appendix. It should be noted, however, that the average minor phase diameter of the 70/30 PS/HDPE blend without SEBS could not be measured because this blend exhibited a co-continuous morphology similar to that shown in a previous study [23]. This difference in blend morphology is in agreement with the known effect [58] of a compatibilizer in an immiscible blend to displace to a higher minor phase volume fraction the transition from a co-continuous blend morphology to a dual-phase blend morphology.

The results presented in Table I indicate that the average particle diameter, which in each blend is less than 1 μm, increases with the HDPE content and that it is not significantly affected by the presence of SEBS for the 5% and 15% minor phase blends. In addition, these results indicate that the average interparticle distance, T, is of the order of 1 μm in the 95/5 PS/HDPE blends, of 0.6 μm in the 85/15 PS/HDPE blends and of 0.3 μm in the 70/30 PS/HDPE blend. These results also indicate that the average number of particles per unit volume increases with the HDPE content, but no clear effect of the presence of SEBS on the morphological characteristics was noted except for the 70/30 PS/HDPE blends. SEM observations [23] showed that the HDPE particles in these injection-moulded PS/HDPE blends, however, are not spherical but rather elongated in the melt-flow direction, and that composite droplets of HDPE with PS subparticles are mostly observed in PS-rich blends with a minor phase content of 15% and 30%. Consequently, the second and third assumptions presented in the Appendix are not strictly valid. The interparticle distance and the particle separation estimates presented in Table I can, however, be considered as the maximum theoretical values of the interparticle distance and the particle separation because the volume fraction of particles is either equal to or higher than the volume fraction of HDPE due to the PS subparticles possibly present in the HDPE particles. Accordingly, the estimates of the number of particles per unit volume presented in Table I can be considered as the minimum theoretical values of the number of particles per unit volume.

3.2. FCP behaviour

FCP tests at increasing ΔK with a constant ΔK-gradient were performed at 2 and 20 Hz for transverse

TABLE I Morphological characterization of the PS/HDPE blends. The HDPE volume fraction, f_a, the average particle diameter, d_a, the average number of particles per unit volume, n_a, the average particle separation, L, the average interparticle distance, T, and the average particle separation to average particle diameter ratio, L/d, are shown

PS/HDPE blend composition	f_a	d_a (μm)	n_a (10^6 mm^{-3})	L (μm)	T (μm)	L/d
95/5 without SEBS	0.054	0.67	340	1.74	1.07	2.6
95/5 with SEBS	0.054	0.62	430	1.62	1.00	2.6
85/15 without SEBS	0.161	0.84	520	1.45	0.61	1.7
85/15 with SEBS	0.162	0.88	450	1.51	0.63	1.7
70/30 with SEBS	0.319	0.94	730	1.21	0.27	1.3

specimens of PS and of 95/5 and 85/15 PS/HDPE with and without SEBS. Tests were also performed at 20 Hz for longitudinal specimens of the same materials. FCP tests were also attempted for longitudinal and transverse specimens of 70/30 PS/HDPE with and without SEBS. Valid FCP curves, however, could not be obtained for the specimens without SEBS as well as for the transverse specimens with SEBS, since a 30°–45° crack deviation from the plane perpendicular to the load axis was systematically obtained for these specimens during precracking. Valid FCP tests were, however, obtained at both 2 and 20 Hz for longitudinal specimens of 70/30 PS/HDPE with SEBS, where some crack deviation from the plane perpendicular to the load axis was also obtained, but where this crack deviation was always less than the 10° crack deviation permitted by ASTM E-647.

The log–log curves of the fatigue crack growth rate, da/dN, versus ΔK are presented in Fig. 2 for pure PS transverse and longitudinal specimens, for the 5% and

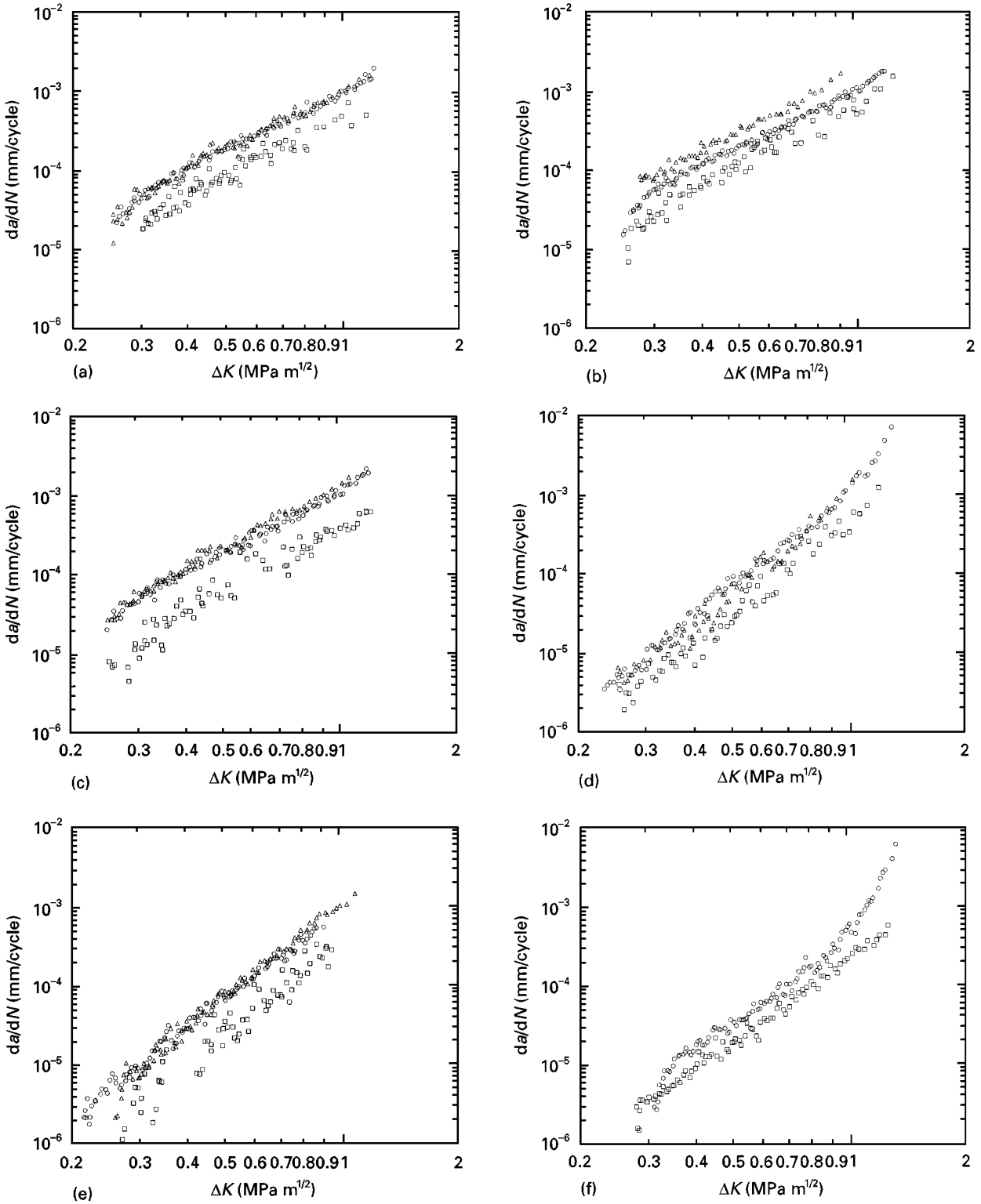

Figure 2 FCP curves showing log da/dN plotted against log ΔK in transverse specimens at (○) 2 Hz and (□) 20 Hz and in longitudinal specimens at (△) 20 Hz of: (a) PS, (b) 95/5 PS/HDPE without SEBS, (c) 95/5 PS/HDPE with SEBS, (d) 85/15 PS/HDPE without SEBS, (e) 85/15 PS/HDPE with SEBS, and (f) 70/30 PS/HDPE longitudinal specimens with SEBS at (○) 2 Hz and (□) 20 Hz.

15% minor phase transverse and longitudinal specimens with and without SEBS, and for the 30% minor phase longitudinal specimens with SEBS. These FCP curves show the well-known constant power-law behaviour or Paris regime [59] described by the relationship

$$\frac{da}{dN} = A\Delta K^n \quad (1)$$

where A and n, which represent, respectively, the ordinate at $\Delta K = 1\ \mathrm{MPa\,m^{1/2}}$ and the slope of a log da/dN–log ΔK plot, are material constants for given test conditions. As shown previously for pure PS and 95/5 PS/HDPE blends [24], the results presented in Fig. 2 indicate that the fatigue crack growth rate increases when the loading frequency is reduced from 20 Hz to 2 Hz for every material tested. These results also indicate that the longitudinal specimens show higher fatigue crack growth rates than the transverse specimens for the same ΔK values. Thus, the specimens loaded parallel to the melt-flow direction during injection moulding (i.e. the transverse specimens) show lower fatigue crack growth rates than the specimens loaded perpendicular to the melt-flow direction (i.e. the longitudinal specimens). These results are in agreement with the higher performance observed in tensile behaviour for these materials when loaded parallel to the melt-flow direction [23].

Power-law regressions were obtained for all the FCP curves. The A and n values calculated from Equation 1 are presented in Table II. The value of the exponent n obtained on specimens of a given material is almost constant, regardless of the loading frequency, the presence of SEBS or the specimen orientation. The average n values obtained were 2.5 for the pure PS specimens, 2.6 for the 95/5 PS/HDPE specimens, 3.8 for the 85/15 PS/HDPE specimens and 3.4 for the 70/30 PS/HDPE specimens. These results therefore indicate that the slope of the Paris regime obtained is considerably influenced by the HDPE content, once this content becomes sufficiently large. The n exponents obtained can be compared with reported n exponents for pure PS and rubber-toughened PS-rich blends of 2.8–4.8 [28, 31, 32, 60].

The results presented in Fig. 2 and Table II also indicate that the fatigue crack growth rate in the FCP specimens increases by an average factor of 2.2 in all materials when the loading frequency is reduced from 20 Hz to 2 Hz. This factor, reflecting the increasing fatigue crack growth rate obtained with decreasing loading frequency, is in agreement with that of 2–2.5 previously reported [24, 28, 32, 41] for PMMA, poly(phenylene oxide)/high impact polystyrene (PPO/HIPS) and PS when the loading frequency was reduced by a factor of ten. From the results presented in Fig. 2 and Table II, an average increase in the fatigue crack growth rate by a factor of 2.7 can be obtained in pure PS, 95/5 and 85/15 PS/HDPE specimens when longitudinal specimens are compared to transverse specimen. No comparison between the fatigue crack growth rates in longitudinal specimens and in transverse specimens can be reported for the 70/30 PS/HDPE blend with SEBS, because the FCP curves of the respective transverse specimens could not be obtained. However, the deviation of the crack in the latter specimens suggests an important reduction in fatigue crack growth rate when going from longitudinal to transverse specimens. This very abrupt and rapid crack deviation can be interpreted as the result of the morphology of the blend and the strong

TABLE II Paris regime parameters, A and n, obtained for pure PS and 95/5 and 85/15 PS/HDPE with or without SEBS, including those of modified CT specimens (i.e. with side grooves present)

Material	Frequency (Hz)	Orientation	A ($\times 10^{-3}$)	n
PS	2	Transverse	1.3	2.6
PS	20	Transverse	0.66	2.6
PS	20	Longitudinal	1.1	2.5
PS[a]	20	Transverse	0.76	2.3
95/5 PS/HDPE without SEBS	2	Transverse	1.1	2.6
95/5 PS/HDPE without SEBS	20	Transverse	0.51	2.6
95/5 PS/HDPE without SEBS	20	Longitudinal	1.8	2.5
95/5 PS/HDPE without SEBS[a]	20	Transverse	0.57	2.2
95/5 PS/HDPE with SEBS	2	Transverse	1.0	2.6
95/5 PS/HDPE with SEBS	20	Transverse	0.35	2.5
95/5 PS/HDPE with SEBS	20	Longitudinal	1.4	2.7
95/5 PS/HDPE with SEBS[a]	20	Transverse	0.55	2.7
85/15 PS/HDPE without SEBS	2	Transverse	0.99	3.9
85/15 PS/HDPE without SEBS	20	Transverse	0.45	3.9
85/15 PS/HDPE without SEBS	20	Longitudinal	0.88	3.9
85/15 PS/HDPE without SEBS[a]	20	Transverse	0.38	3.5
85/15 PS/HDPE with SEBS	2	Transverse	0.88	3.7
85/15 PS/HDPE with SEBS	20	Transverse	0.36	3.8
85/15 PS/HDPE with SEBS	20	Longitudinal	0.85	3.8
85/15 PS/HDPE with SEBS[a]	20	Transverse	0.71	3.7
70/30 PS/HDPE with SEBS	2	Longitudinal	0.36	3.4
70/30 PS/HDPE with SEBS	20	Longitudinal	0.20	3.4

[a]Modified CT specimens.

orientation effect on the FCP behaviour of injection-moulded specimens, in agreement with previous results [23, 24].

The average A values in Table II also indicate that the addition of HDPE to PS affects the FCP resistance of the specimens. At an HDPE content of 5%, the transverse specimens with and without SEBS show a slight fatigue crack growth rate reduction by an approximately constant factor of 1.3 when compared to pure PS specimens. On the other hand, the corresponding longitudinal specimens show a fatigue crack growth rate increase with respect to the corresponding PS specimens by an approximately constant factor of 1.7 in the 95/5 PS/HDPE blends without SEBS and by a small factor, which progressively increases from 1.0 at low ΔK to 1.3 near the highest ΔK employed in the tests, in the 95/5 PS/HDPE blends with SEBS.

For minor phase contents of 15% and 30%, however, the fatigue crack growth rate reduction is considerably more important, with the fatigue crack growth rate reduction factor (i.e. the ratio between the fatigue crack growth rate in PS and the fatigue crack growth rate in the blends) for these blends shown in Fig. 3. The fatigue crack growth rate reduction caused by the addition of 15% minor phase to PS progressively decreases from an average factor of 8.2 at low ΔK to an average factor of 1.3 near the final ΔK. In the case of the 70/30 PS/HDPE longitudinal specimens with SEBS, the fatigue crack growth rate reduction decreases from an average factor of 20 at low ΔK to an average factor of 6 near the final ΔK. This progressive change in the fatigue crack growth rate reduction factor of these PS/HDPE specimens compared to PS specimens is in agreement with the values of A and the n exponents reported in Table II when 15% and 30% minor phase is added to PS. The K_{max} values at failure (i.e. those associated with the transition from the Paris fatigue crack growth regime to the final fracture regime) did not appear to be increased by minor phase addition (Fig. 2). Because most of the life before failure during FCP is generally determined by the fatigue crack growth rates at low ΔK [2], the FCP resistance in most practical applications would be considerably increased in a compatibilized 70/30 PS/HDPE blend when compared to pure PS and other PS-rich PS/HDPE blends of lower minor phase content. That the fatigue crack growth rate is almost unchanged by the presence of the minor phase at high ΔK is also in agreement with the relatively poor toughening effects observed in these blends during higher speed fracture tests in monotonic loading, such as tensile testing [23], impact testing [61], and fracture toughness (K_{Ic} or K_c) testing [62]. Furthermore, these results demonstrate that fatigue properties of such materials cannot be estimated from monotonic loading tests, such as impact tests.

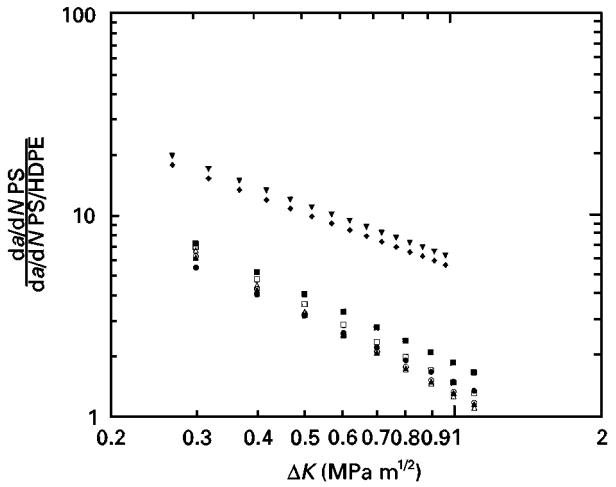

Figure 3 Ratio between the fatigue crack growth rate in PS and in PS/HDPE plotted against ΔK on a log–log scale for 85/15 transverse specimens with or without SEBS cycled at (○, ●) 2 Hz and at (□, ■) 20 Hz, and in longitudinal specimens cycled at (△, ▲) 20 Hz and in 70/30 longitudinal specimens with SEBS cycled at (▼) 2 Hz and at (◆) 20 Hz. (○, □, △) blends without SEBS, (●, ■, ▲, ▼, ◆) blends with SEBS.

As also shown in Table II, the variation of the A values when specimens with SEBS are compared to specimens without SEBS indicates that the addition of SEBS to PS/HDPE blends generally leads to a small but significant reduction of the fatigue crack growth rates for a given testing condition. In addition, the A values presented in Table II indicate that the modified CT specimens, in which a 0.45 mm deep layer at each lateral surface was removed along the expected fracture plane (in order to remove the highly oriented skin), also affected the FCP behaviour. When the oriented skin was removed, a general increase of the fatigue crack growth rates of transverse specimens by an average factor of 1.3 in pure PS, of 1.4 in 95/5 PS/HDPE with and without SEBS, and of 2.1 in 85/15 PS/HDPE with SEBS, was obtained. However, removing the skin on 85/15 PS/HDPE transverse specimens without SEBS showed little effect on the fatigue crack growth rates.

3.3. Fractographic observations

The FCP fracture surfaces of the transverse specimens of pure PS as well as those of 95/5 PS/HDPE blends with and without SEBS have been previously described [24]. The fracture surface of pure PS specimens presented DGBs at low fatigue crack growth rates (typically up to $1–2 \times 10^{-4}$ mm/cycle), "large" dimple-like features, 1–3 μm diameter, at medium da/dN (typically from $1–2 \times 10^{-4}$ mm/cycle to $3–4 \times 10^{-4}$ mm/cycle) and fatigue striations at high da/dN (typically greater than $3–4 \times 10^{-4}$ mm/cycle). The large dimple-like features at medium fatigue crack growth rates had initiated as one or several small microvoids near the centre of the large dimple (but generally closer to the side of the previous crack front) and had then grown into the large dimple in part by coalescence with other small microvoids near the edges of the growing large dimple. The large dimples were approximately aligned into bands parallel to the DGBs and to the striations. The size of these dimples initially increased as the fatigue crack growth rates increased. At higher fatigue crack growth rates, however, such large dimples became interspersed with the striations, with fewer large dimples being observed with increasing fatigue crack growth rates.

The fracture surfaces of the 95/5 PS/HDPE specimens presented DGBs at low fatigue crack growth rates (typically up to $1–2 \times 10^{-4}$ mm/cycles, which could be recognized by the presence of microvoids near their start, many of which had not formed at HDPE particles. At medium fatigue crack growth rates (typically from $1–2 \times 10^{-4}$ mm/cycle to $3–4 \times 10^{-4}$ mm/cycle), the fracture surface presented groups of large dimples, 0.5–3 μm diameter, more or less aligned in bands. Most of these dimples had initiated as a microvoid around an HDPE particle, as indicated by the presence of small U-shaped microvoids pointing towards the HDPE particle at which the large dimple initiated (Fig. 4a). These dimple-like features all had grown in part by coalescence with these small U-shaped microvoids. For fatigue crack growth rates greater than approximately $3–4 \times 10^{-4}$ mm/cycle, the fracture surfaces again presented DGBs as well as groups of dimples aligned parallel to the DGBs (Fig. 4b). As the fatigue crack growth rates increased, these groups of dimples became progressively less continuous and less numerous until they finally disappeared. Many of the HDPE particles present in the fracture surface near the start of the DGBs were noticeably elongated, indicating that they had been strongly stretched during crack propagation, while HDPE particles present in the middle of the DGB's were usually not noticeably elongated.

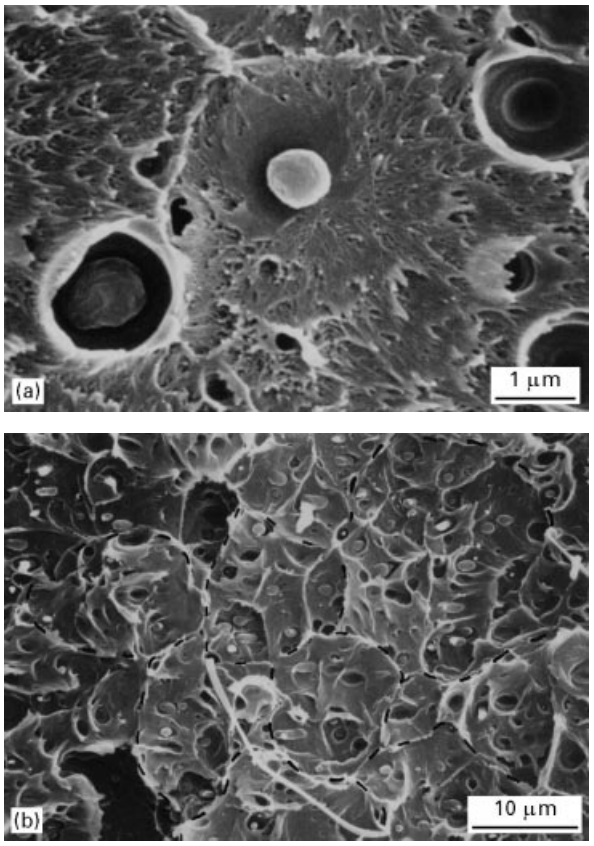

Figure 4 (a) Micrograph showing a large dimple-like feature formed around an HDPE particle in a non-compatibilized 95/5 PS/HDPE specimen for $\Delta K = 0.65$ MPa $m^{1/2}$, $da/dN = 3.6 \times 10^{-4}$ mm/cycle and $f = 2$ Hz. Fine U-shaped microvoids pointing towards the HDPE particle located in the centre of the micrograph at which this large dimple initiated can be observed. (b) Micrograph showing groups of dimples (dashed line), approximately 10 μm diameter, aligned parallel to the DGBs in a compatibilized 95/5 PS/HDPE specimen for $\Delta K = 1.0$ MPa $m^{1/2}$, $da/dN = 1.0 \times 10^{-3}$ mm/cycle and $f = 2$ Hz. The macroscopic FCP direction is, in both cases, from left to right.

In addition, a loading frequency effect was also noted on the fracture surfaces of the PS specimens and 95/5 PS/HDPE specimens [24]. When the loading frequency was decreased from 20 Hz to 2 Hz in PS and 95/5 PS/HDPE specimens, fractographic observations indicated that the number of dimples not associated with HDPE particles in the DGBs as well as the number of both non-elongated and elongated particles in the DGBs increased. These observations indicate that the effect of the loading frequency is associated with a time-dependent deformation process, similar to a creep effect, resulting from the load application time increasing when the loading frequency is reduced.

In the present study, the FCP fracture surfaces of the 85/15 and 70/30 PS/HDPE specimens with and without SEBS were observed. Stereographic observations of the fracture surfaces of the 85/15 PS/HDPE transverse specimens with and without SEBS indicated the presence of the DGBs for the whole range of fatigue crack growth rates measured (Fig. 5a–d). In addition, somewhat elongated HDPE particles in the specimens without SEBS (Fig. 5a) and very elongated HDPE particles in the specimens with SEBS (Fig.5d) were observed, indicating an increased particle–matrix adhesion in the presence of SEBS. In agreement with previous observations in 95/5 PS/HDPE specimens [24], detailed stereofractographic observations indicated that these elongated particles were usually more numerous near the start of the DGBs than in the remaining portion of the DGBs (Fig. 5). This feature, in turn, could be employed to help recognize the position of the DGBs. The presence of ridge lines parallel to the FCP direction at low fatigue crack growth rates was also noted (Fig. 5a). These lines generally initiated at elongated HDPE particles near the start of the DGBs and then continued for some distance following the crack propagation direction. The breaks and jogs observed on these ridge lines were frequently aligned, which also helped to identify the positions at which the DGBs started. As the fatigue crack growth rate increased, these ridge lines became rarer. The elongation of the HDPE particles was found to increase when the fatigue crack growth rates increased (Fig. 5a–c), indicating an increased plastic deformation of the HDPE particles, at least near the start of the DGBs, as ΔK increased. Although less important in the presence of SEBS (Fig. 5d), a relatively large proportion of the HDPE particles on the fracture surfaces were not noticeably elongated, indicating for such particles a significant amount of decohesion at the particle–matrix interface.

Relatively large features, polygonal or very roughly rectangular in shape (Fig. 5a, b, d and Fig. 6), typically 10–20 μm long and wide, were also observed on the fracture surfaces of the 85/15 PS/HDPE specimens throughout the DGBs. At low fatigue crack growth rates, these features corresponded to flat regions in the PS matrix (Fig. 5a) closely similar in the FCP

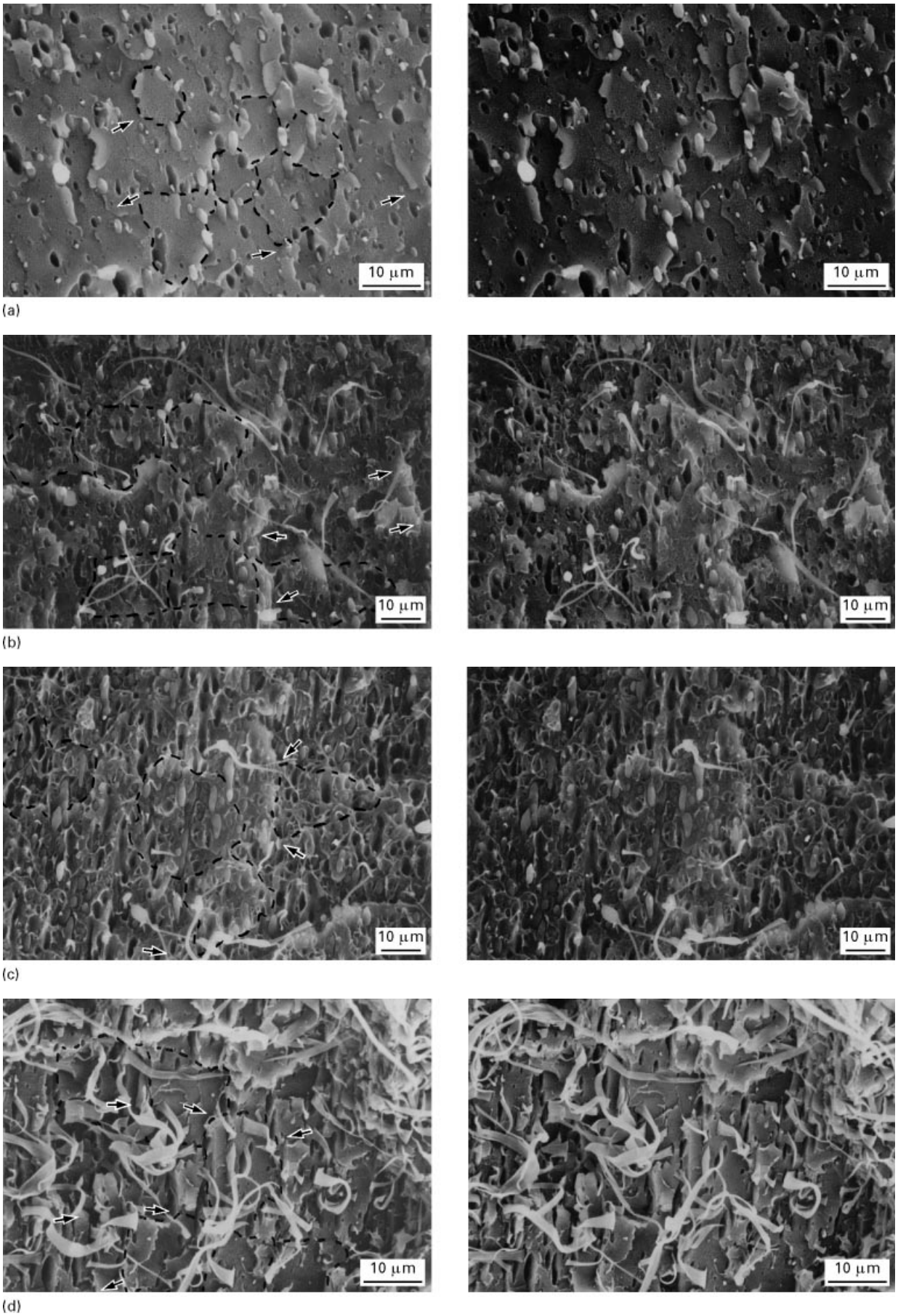

Figure 5 Stereofractographs of DGBs with polygonal features present observed in 85/15 PS/HDPE transverse specimens, (a) without SEBS ($\Delta K = 0.26$ MPa $m^{1/2}$, $da/dN = 2.5 \times 10^{-6}$ mm/cycle, 20 Hz and DGB width ≈ 7 μm, (b) without SEBS ($\Delta K = 0.69$ MPa $m^{1/2}$, $da/dN = 1.1 \times 10^{-4}$ mm/cycle, 20 Hz and DGB width ≈ 16 μm), (c) without SEBS ($\Delta K = 1.15$ MPa $m^{1/2}$, $da/dN = 7.8 \times 10^{-4}$ mm/cycle, 20 Hz and DGB width ≈ 23 μm),(d) with SEBS ($\Delta K = 0.86$ MPa $m^{1/2}$, $da/dN = 2.0 \times 10^{-4}$ mm/cycle, 20 Hz and DGB width ≈ 16.0 μm). The arrows indicate some of the breaks and jogs of the ridges lines when visible and the dashed lines indicate some of the polygonal features. The macroscopic FCP direction is from top to bottom.

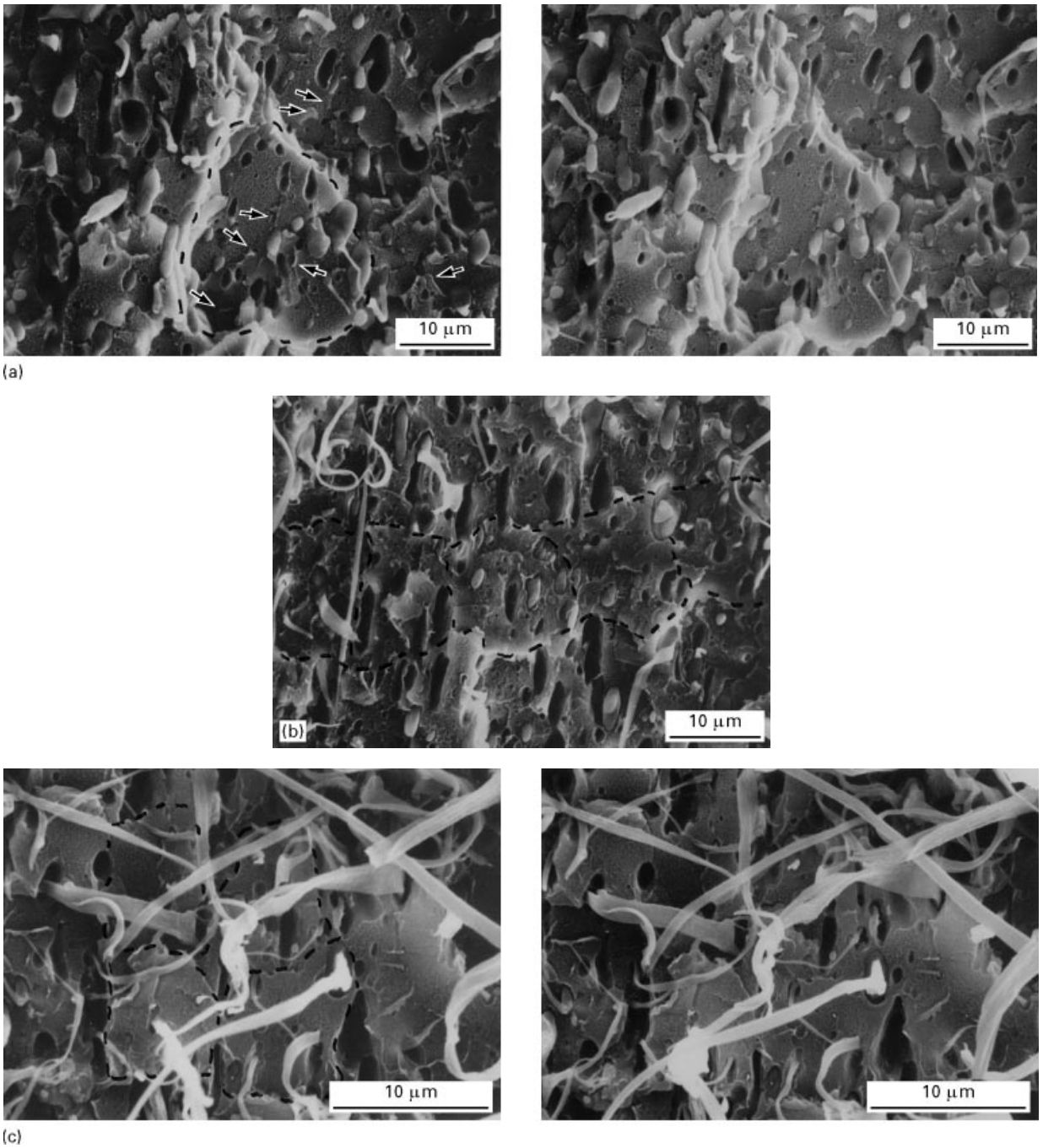

Figure 6 (a) Stereofractographs of a region showing a polygonal feature, 20 μm in width, observed in a 85/15 PS/HDPE transverse specimen without SEBS ($\Delta K = 0.49$ MPa $m^{1/2}$, $da/dN = 3.0 \times 10^{-5}$ mm/cycle and 20 Hz), (b) DGBs, 25 μm in width, observed in a 85/15 PS/HDPE transverse specimen without SEBS ($\Delta K = 0.63$ MPa $m^{1/2}$, $da/dN = 8.0 \times 10^{-5}$ mm/cycle and 20 Hz) formed by the coalescence of polygonal features; (c) large and flat polygonal features, in which very elongated HDPE particles are present, observed in a 70/30 PS/HDPE transverse specimen with SEBS ($\Delta K = 0.69$ MPa $m^{1/2}$, $da/dN = 5.0 \times 10^{-5}$ mm/cycle and 20 Hz). The arrows indicate some of the ridge lines radiating in every direction from HDPE particles when visible, and the dashed lines, some of the polygonal features. The macroscopic FCP direction is from top to bottom.

direction to the DGBs observed in the PS specimens and in the 95/5 PS/HDPE specimens at similar fatigue crack growth rates [24]. Also, the presence of elongated HDPE particles within these large and flat features away from their edges became more numerous as the fatigue crack growth rates increased. At times, small ridge lines radiated in every direction from these elongated particles (Fig. 6a), indicating that these polygonal features had formed ahead of the previous local crack tip in the crazed zone. These small ridge lines were increasingly present in the polygonal features as the fatigue crack growth rates increased. At intermediate and high fatigue crack growth rates, these features became increasingly less flat and took on more of an appearance of large dimples in which several HDPE particles were present. At high ΔK, the small ridge lines also became uniformly present.

Similar polygonal features (Fig. 6c), containing several HDPE particles as well as ridge lines radiating in every direction from these particles, were observed in the 70/30 PS/HDPE longitudinal specimens with SEBS. As in the 85/15 PS/HDPE specimens (Fig. 6b), these ridge lines indicated that the polygonal features had formed in the crazed zone in front of the local

crack tip. Again, the initiation, growth and coalescence of these features in the craze zone led to DGB formation, similar to the multiple crazing effect observed in static loading in rubber-toughened specimens. In the 70/30 PS/HDPE longitudinal specimens with SEBS, these polygonal features were observed for the whole range of fatigue crack growth rates obtained, not only at low or moderate fatigue crack growth rates, as in the 85/15 PS/HDPE specimens. The HDPE particles, however, became increasingly elongated with increasing fatigue crack growth rate as a result of the increasing deformation, making it progressively more difficult to observe the polygonal features on the fracture surface of the PS matrix for these 70/30 PS/HDPE specimens with SEBS.

The large dimple-like features, 0.5–3 μm diameter, observed in the 95/5 PS/HDPE specimens at intermediate and high ΔK (Fig. 4), although smaller in diameter, presented an important similarity with the polygonal features, 10–20 μm diameter, observed in the 85/15 and 70/30 PS/HDPE specimens. In effect, both type of feature initiated ahead of the previous crack tip in the crazed zone and were formed by the initiation, growth and coalescence of microvoids around HDPE particles. The fracture of the dimple-like features, however, generally initiated at a single HDPE particle, while the fracture of the polygonal features generally initiated at several HDPE particles.

Re-examination of the DGBs on the high fatigue crack growth rate portion of the fracture surfaces of the 95/5 PS/HDPE specimens also showed many polygonal regions 10–20 μm in size containing groups of dimples of approximately 3 μm diameter (Fig. 4b). These dimples were quite similar to those observed at intermediate fatigue crack growth rates, except that at high fatigue crack growth rates, there was neither an interface separating the dimples from each other nor were there small U-shaped dimples observable which had not formed at HDPE particles. These observations thus indicate that, for sufficiently high fatigue crack growth rates, the DGB formation in the blends occurs by a multiple crazing effect with crack initiation at HDPE particles. This multiple crazing appears similar to that observed during monotonic loading in rubber-toughened blends [63] and occurs starting from lower fatigue crack growth rate values as the volume percentage occupied by HDPE particles increases in blends in which particles of HDPE are contained within a PS matrix. The observations also strongly suggest that the dimpled fracture observed between approximately $1–2 \times 10^{-4}$ and $3–4 \times 10^{-4}$ mm/cycle in the 95/5 PS/HDPE blends occurs simply because there is an insufficient amount of HDPE particles in these blends to change the behaviour at these fatigue crack growth rates from that observed in PS to that observed in the blends with greater amounts of HDPE.

The precrack fracture surfaces of the 70/30 PS/HDPE longitudinal and transverse specimens without SEBS, showing a co-continuous morphology, were observed in order to understand better the important precrack deviation obtained. For both orientations, the precrack deviated toward a plane approximately at 45° to the melt-flow direction. Observations of the fracture surfaces showed easy decohesion at the PS–HDPE interface. In addition, an apparent progressive change from a coarse co-continuous morphology to an oriented co-continuous morphology parallel to the FCP direction was noted on the precrack fracture surfaces as the crack deviation increased (Fig. 7).

The precrack fracture surfaces of the 70/30 PS/HDPE transverse specimens with SEBS were also observed. An increasingly apparent minor phase domain size and aspect ratio were noted on the fracture surfaces as the deviation of the precrack increased in importance (Fig. 8). Because no significant variation of the minor phase domain size and orientation was noted in the CT specimens employed for a given orientation, such an increase in the apparent minor phase domain size suggests that the fatigue precrack was deviated progressively by the presence of the elongated minor phase domains aligned parallel to the melt-flow direction and perpendicular to the intended crack propagation plane. This observation indicates that the presence of aligned minor phase domains with important length-to-width ratios can constitute an effective barrier to FCP, at least at the low ΔKs employed during fatigue precracking. A strong orientation effect of the blend morphology on the FCP

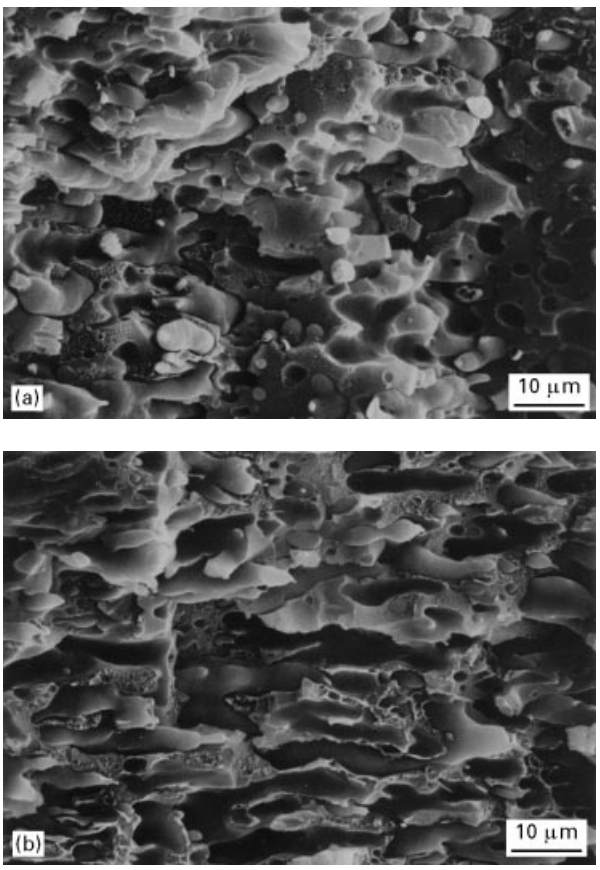

Figure 7 Fractographs observed in a 70/30 PS/HDPE transverse specimen without SEBS, (a) after approximately 0.8 mm precrack propagation (crack deviation < 5°) showing a coarse and non-oriented co-continuous morphology, (b) after approximately 4.0 mm precrack propagation (crack deviation > 30°) showing an oriented co-continuous morphology parallel to the FCP direction. The macroscopic FCP direction is from left to right.

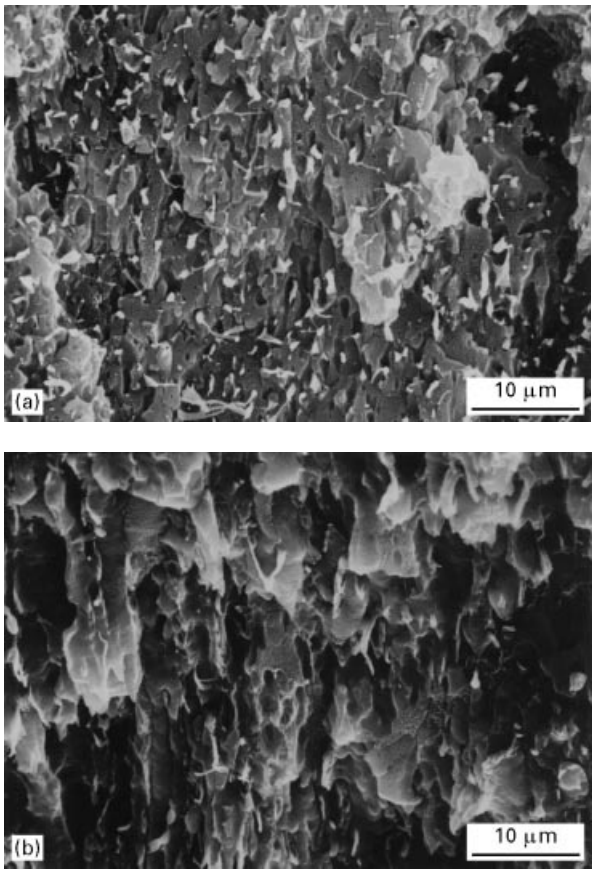

Figure 8 Fractographs observed in a 70/30 PS/HDPE transverse specimen with SEBS (a) after approximately 0.3 mm precrack propagation (crack deviation $< 5°$) showing a very fine minor phase distribution, (b) after approximately 6.2 mm precrack propagation (crack deviation $\approx 45°$) showing a very oriented and elongated minor phase morphology parallel to the FCP direction. The macroscopic FCP direction is from top to bottom.

behaviour of injection-moulded specimens then results, in agreement with previous results [23, 24].

Interestingly, the specimens showing the highest average particle diameter and the lowest average particle separation to average particle diameter ratio, i.e. the specimens of 70/30 PS/HDPE with SEBS (Table I), correspond to those showing the lowest fatigue crack growth rate. This is in agreement with the morphological criteria based on the average particle diameter (2–5 μm [63–69]) and on the average particle separation to average particle diameter ratio ($L/d < 1.45$ [70]) proposed to obtain a significant toughening effect from multiple crazing in static loading. Thus, this suggests that the formation of the polygonal features leading to the DGB formation is associated with an important reduction of the fatigue crack growth rate in FCP at a given ΔK, similar to the multiple crazing effect observed in static loading in rubber-toughened specimens. Although less important than in the 70/30 PS/HDPE longitudinal specimens with SEBS, a significant fatigue crack growth rate reduction was also obtained in the 85/15 PS/HDPE specimens when the formation of the polygonal features was observed (i.e. at low and moderate ΔK), again suggesting that the formation of such features is associated with an important fatigue crack growth rate reduction.

As mentioned previously for the 95/5 PS/HDPE specimens [24], fractographic observations also indicated that, when the loading frequency was changed from 20 Hz to 2 Hz, the elongation of the HDPE particles on the fatigue surfaces of the 85/15 and 70/30 PS/HDPE specimens increased, suggesting an effect of loading frequency associated with a time-dependent deformation process. However, the very high number of HDPE particles on the fracture surfaces, as well as their very important elongation in the latter two compositions, made it essentially impossible to determine whether the number of dimples or the number of particles in the DGBs was modified by such a change in loading frequency.

The FCP fracture surfaces of longitudinal specimens of pure PS, 95/5 and 85/15 PS/HDPE blends without SEBS were also observed. No significant differences in the fracture surfaces of either the PS or the 95/5 PS/HDPE longitudinal and transverse specimens was noted. DGBs were observed on the fracture surfaces of the blend specimens for the whole range of fatigue crack growth rates (Fig. 9). Also, the presence of ridge lines parallel to the FCP direction, which generally initiated at these elongated particles near the start of the DGBs and then continued for some distance following the crack propagation direction, was also noted. The breaks and jogs observed on these ridge lines were frequently aligned, which also helped to identify the start of the DGBs. However, the fracture surfaces of 85/15 PS/HDPE specimens showed the presence of fibre-like HDPE particles in the longitudinal specimens and only slightly elliptical HDPE particles in the transverse specimens (Figs 5 and 6), as a result of the morphological effect induced by the injection-moulding process [23]. The elongated HDPE particles on the fracture surfaces in the longitudinal specimens, moreover, were considerably more elongated, probably due to their initial morphology after injection moulding, than the particles in the transverse specimens. In agreement with the tensile behaviour of pure PS and PS/HDPE blends [23],

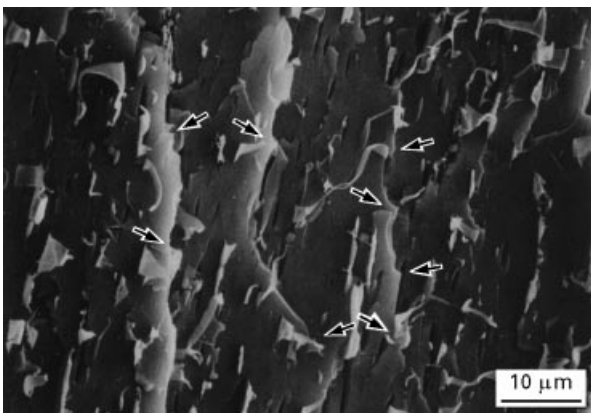

Figure 9 Fractographs of DGBs (approximately 8.5 μm in width) observed in a 85/15 PS/HDPE longitudinal specimen without SEBS at a loading frequency of 20 Hz, $\Delta K = 0.27$ MPa $m^{1/2}$ and $da/dN = 5.0 \times 10^{-6}$ mm/cycle showing very oriented and elongated HDPE particles. The arrows indicate some of the breaks and jogs of the ridges lines when visible. The macroscopic FCP direction is from top to bottom.

these specimens showed lower fatigue crack growth rates when loaded parallel to the average matrix and particle orientation.

3.4. DGB measurements

SEM stereographic observations of the fracture surfaces were employed to measure the DGB width. These measurements were performed for PS as well as for compatibilized and non-compatibilized 95/5 and 85/15 PS/HDPE transverse specimens tested at loading frequencies of 2 and 20 Hz, for PS and for 95/5 and 85/15 PS/HDPE non-compatibilized longitudinal specimens tested at a loading frequency of 20 Hz, and for compatibilized 70/30 PS/HDPE longitudinal specimens tested at 2 and 20 Hz. The DGB width measurements plotted against ΔK on a log–log scale are shown in Fig. 10. Because DGBs in pure PS specimens are only observed at low and moderate fatigue crack growth rates, Fig. 10 shows a limited range of DGB width measurements for these specimens. In PS/HDPE blends, however, DGBs continue to be observed to higher ΔK until final fracture, although, for the 95/5 PS/HDPE specimens, large dimple-like features were observed at intermediate fatigue crack growth rates. In agreement with previous results [24], those presented in Fig. 10 indicate that the DGB width varies with ΔK^i, with the calculated i exponent varying between 1.0 and 1.6 in pure PS specimens, between 0.5 and 0.7 in 95/5 PS/HDPE specimens with and without SEBS, between 0.6 and 0.9 in 85/15 PS/HDPE specimens with and without SEBS, and being approximately equal to 0.8 in 70/30 PS/HDPE specimens with SEBS. Thus, in agreement with results reported in previous studies [71–74], the relationship between the DGB width and ΔK does not appear to correspond to the plastic zone size inferred from the Dugdale model [75], which should result in an i exponent of 2. The fracture surface of the 70/30 PS/HDPE specimens was partly hidden by the very important surface density of highly elongated HDPE particles (Table II), which complicated the observation of the DGBs even when stereographic fractographs were employed. The DGBs observed in the 70/30 PS/HDPE specimens to obtain DGB width measurements corresponded to the clearest and widest DGBs in a given area of the fracture surface. Narrower DGBs could be found with more difficulty. The DGB width measurements presented in Fig. 10d for 70/30 PS/HDPE specimens therefore probably involve a certain overestimation. Nevertheless, these results were reproducible from one area to another.

These results also indicate that the DGB width increases by an average factor of 1.5, for the same ΔK

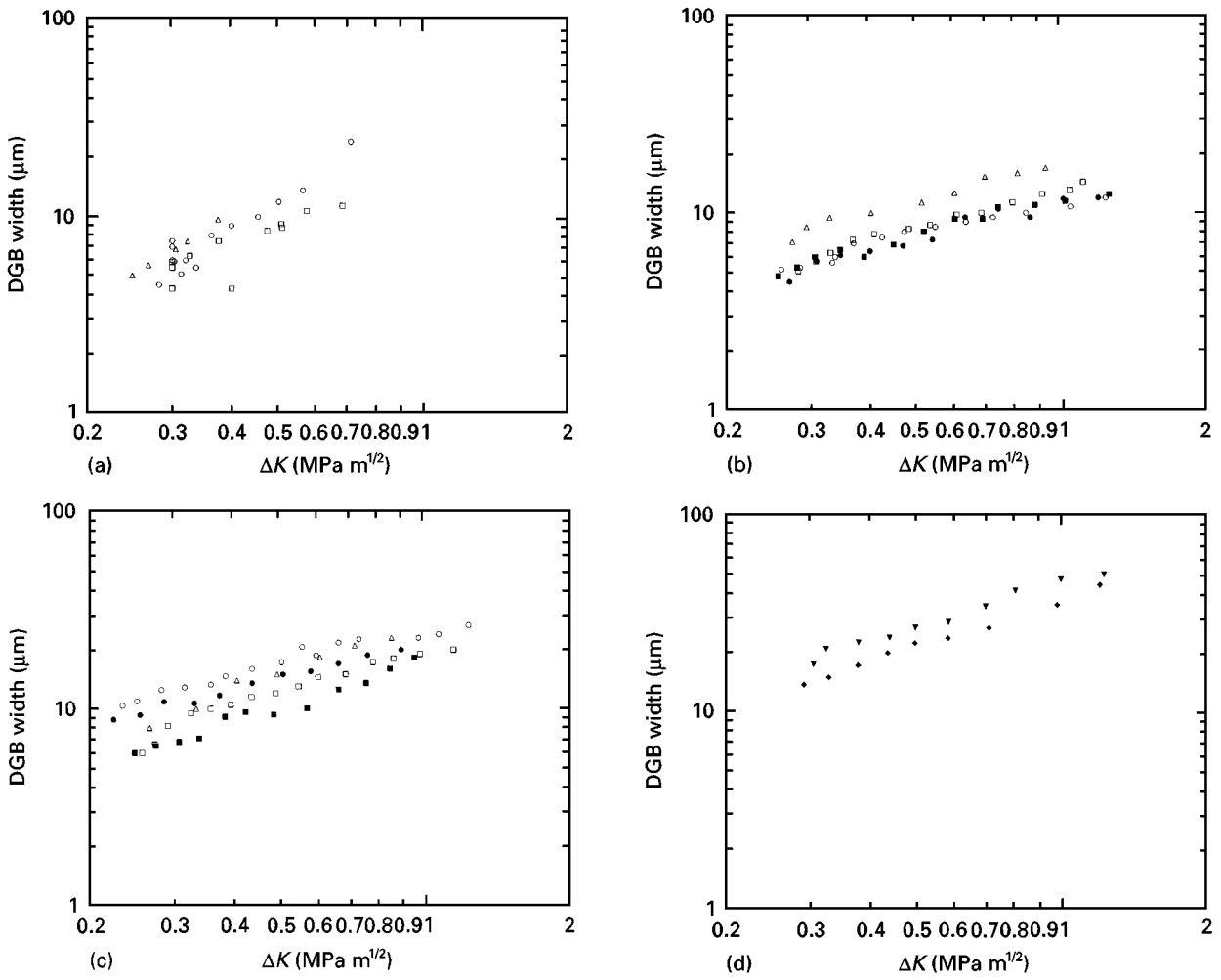

Figure 10 DGB width plotted against ΔK on a log–log scale in transverse specimens at (○, ●) 2 Hz and (□, ■) 20 Hz and in longitudinal specimens at (△) 20 Hz of (a) PS, (b) 95/5 PS/HDPE, (c) 85/15 PS/HDPE, as well as (d) in longitudinal specimens of 70/30 PS/HDPE with SEBS at (▼) 2 Hz and (◆) 20 Hz. (○, □, △) blends without SEBS, (●, ■, ▼, ◆) blends with SEBS.

value, in PS specimens and in 85/15 and 70/30 PS/HDPE specimens when the loading frequency is reduced from 20 Hz to 2 Hz. The 95/5 PS/HDPE specimens, however, do not show as significant a variation in the DGB width for the variation of loading frequency employed. These results, nevertheless, suggest that the plastically strained craze zone, associated with DGB formation, decreases in size when the loading frequency is increased, in disagreement with the expected increase in the size of the DGBs associated with a localized heating effect, which has been previously proposed [32] to explain the fatigue crack growth rate decrease when the loading frequency increases. On pure PS and 95/5 PS/HDPE specimens [24], infrared spectroscopy and thermocouples inserted into specimens during FCP tests did not show any significant temperature rise in the crack-tip region. Also, only a very weak secondary viscoelastic transition was observed in these materials for the FCP test conditions [24]. This decrease in DGB width is, however, in agreement with the previous results [24] on the microfractographic features of the DGBs and on the deformation of the HDPE particles in the DGBs when the loading frequency is changed. In both cases, these results indicate that the fatigue crack growth rate decrease, observed in these blends when the loading frequency is increased, is associated with a decrease in the non-elastic strain per cycle (i.e. a reduction of the fatigue damage per cycle), which is a time-dependent or strain rate-dependent effect. This non-elastic strain per cycle is the factor normally expected to control the fatigue crack growth rate in a ductile material.

Fig. 11 presents N_{DGB}, the number of cycles associated with the formation of a single DGB, plotted against ΔK on a log–log scale. This variable was chosen to characterize the resistance to DGB formation (i.e. the number of fatigue cycles required for DGB formation) because a discussion of the DGB formation resistance based simply on the DGB width would take into account neither the velocity of the macroscopic crack nor the number of cycles until the failure of all or part of the craze, resulting in the formation of a DGB. For example, the DGB width of non-compatibilized 85/15 PS/HDPE transverse specimens uniformly increases by a factor of approximately 1.4 when the loading frequency is reduced from 20 Hz to 2 Hz. However, an increase in the fatigue crack growth rates by a factor of approximately 2.2 was observed in these blends for this decrease in loading frequency. Although the DGBs appear larger at a given ΔK at 2 Hz than at 20 Hz, the results in Fig. 11 clearly show that the DGB formation resistance (i.e. N_{DGB}) in these specimens increases when the loading

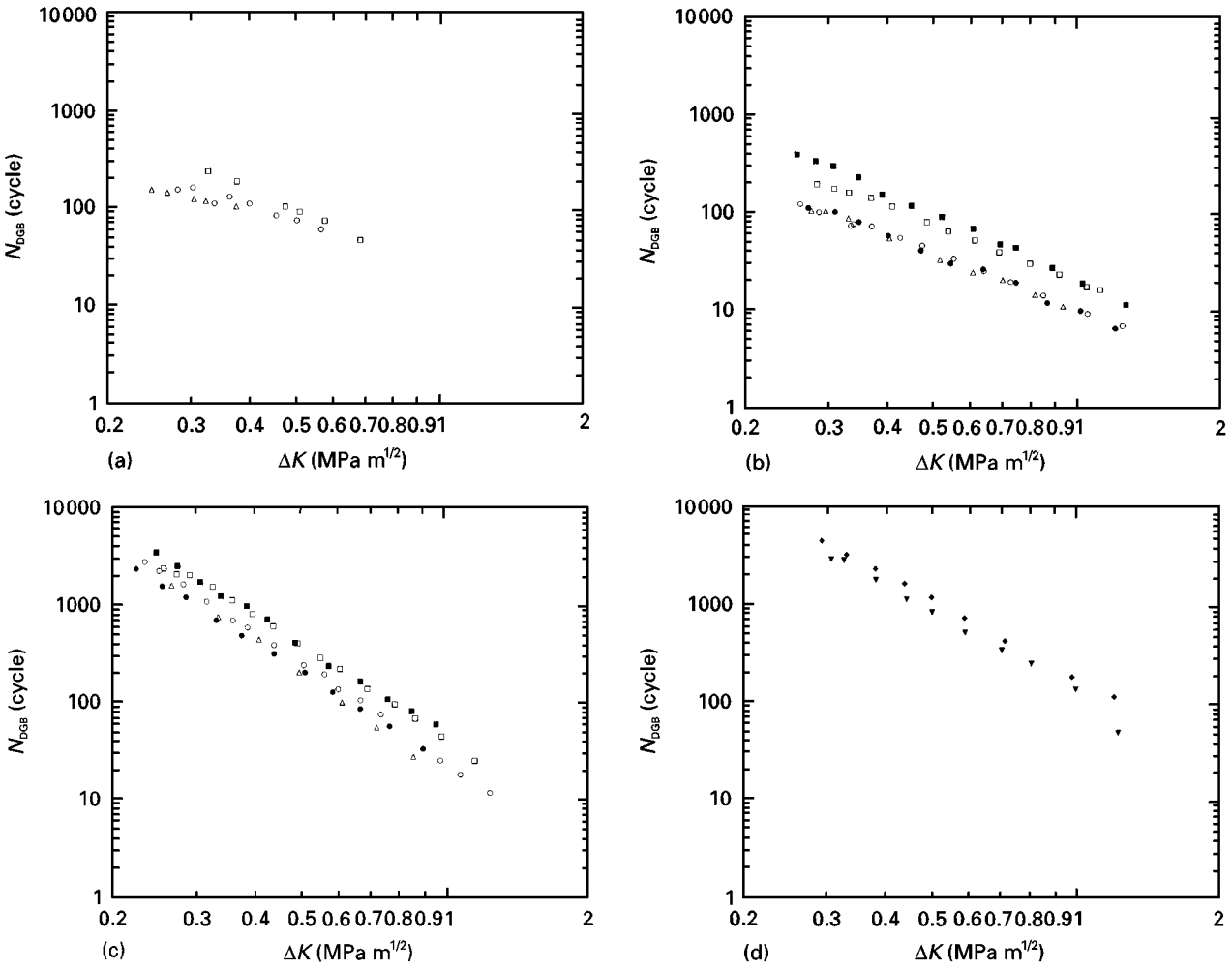

Figure 11 N_{DGB} plotted against ΔK on a log–log scale in transverse specimens at (○, ●) 2 Hz and (□, ■) 20 Hz and in longitudinal specimens at (△) 20 Hz of (a) PS, (b) 95/5 PS/HDPE, (c) 85/15 PS/HDPE, as well as (d) in longitudinal specimens of 70/30 PS/HDPE with SEBS at (▼) 2 Hz and (◆) 20 Hz. (○, □, △) blends without SEBS, (●, ■, ▼, ◆) blends with SEBS.

frequency is increased from 2 Hz to 20 Hz. This increase in the DGB formation resistance by an approximate factor of 1.9 from the results presented in Fig. 11 can be compared to the fatigue crack growth rate reduction by a factor of 2 to 2.5 for the same variation of loading frequency employed.

These results also indicate that the transverse specimens show higher DGB formation resistance than the longitudinal specimens for every material tested. Moreover, the DGB formation resistance appears similar in pure PS specimens and in 95/5 PS/HDPE specimens. In 85/15 PS/HDPE specimens, however, the DGB formation resistance increases by a factor of almost 10 at low ΔK and by a factor of approximately 2 near the final ΔK when compared to pure PS or 95/5 PS/HDPE specimens. In addition the DGB formation resistance in the 70/30 PS/HDPE longitudinal specimens with SEBS increases by an approximate factor of 31 at low ΔK progressively decreasing to an approximate factor of 2 near the final ΔK when compared to pure PS specimens. Moreover, the DGB formation resistance is either unaffected or only slightly increased when SEBS is added to HDPE in 95/5 and 85/15 PS/HDPE specimens. Because no valid FCP results could be obtained in 70/30 PS/HDPE specimens without SEBS, this effect of SEBS could not be verified for this composition. Nevertheless, the DGB formation in PS/HDPE blends is only beneficial to the FCP behaviour when the DGB formation resistance is increased. Consequently, the condition showing the highest DGB formation resistance, i.e. the compatibilized 70/30 PS/HDPE longitudinal specimens, provides the lowest fatigue crack growth rates obtained at a given ΔK value.

4. Conclusions

1. An increase in the HDPE content in PS-rich PS/HDPE blends leads to a reduction of the fatigue crack growth rates, with this reduction being larger when SEBS is added as a compatibilizer.

2. An increase in the loading frequency in such blends also leads to a reduction of the fatigue crack growth rates in the blends.

3. The fatigue crack growth rates are lower at a given ΔK when the injection-moulded specimens are tested parallel, instead of normal, to the melt-flow direction.

4. DGBs, associated with the fracture of crazes formed in the plastic zone, are present throughout the fatigue portion of the fracture surfaces of the PS/HDPE specimens, except at intermediate fatigue crack growth rates in 95/5 PS/HDPE specimens.

5. At sufficiently high fatigue crack growth rates, these DGBs are formed by the initiation, growth and coalescence of large dimples initiated at HDPE particles ahead of the microscopic crack front in PS/HDPE specimens, similar to the multiple crazing effect generally observed in monotonic loading in rubber-toughened specimens.

6. The DGB width varies with ΔK^i where the i exponent is approximately 1–1.6 in PS specimens, 0.5–0.7 in 95/5 PS/HDPE specimens, 0.6 to 0.9 in 85/15 PS/HDPE specimens and 0.8 in 70/30 PS/HDPE specimens.

7. The width of the DGBs as well as the deformation of the HDPE particles in the DGBs increase when the loading frequency is reduced from 20 Hz to 2 Hz.

8. The fractographic observations suggest that the loading frequency effect on the fatigue crack growth rates in the PS/HDPE specimens is related to a time-dependent deformation process, similar to a creep effect, in which the load application time per cycle increases when the frequency is reduced, and therefore increases the fatigue damage per cycle.

Finally, the FCP behaviour of PS/HDPE blends is strongly affected by the loading direction, the matrix and minor phase orientation, the presence of a compatibilizer, the blend composition and morphology, and the testing conditions.

Acknowledgements

Financial assistance from the NSERC (Canada) and FCAR (Québec) research support programmes is gratefully acknowledged.

Appendix

The surface-to-surface interparticle distance, T, and the centre-to-centre particle separation, L, were calculated assuming that the particles are uniformly distributed, that each particle is represented by a sphere, and that the particles are homogeneous and are exclusively composed of HDPE. Thus, to each HDPE particle of diameter, d_a, corresponds a PS sphere of diameter, d_b, such that

$$\begin{aligned} n_a &= n_b \\ &= n \end{aligned} \tag{A1}$$

where n_a and n_b are, respectively, the number of HDPE and PS spheres per unit volume, V. Consequently, the HDPE volume, V_a, is given by

$$\begin{aligned} V_a &= f_a V \\ &= n \frac{\pi}{6} d_a^3 \end{aligned} \tag{A2}$$

If $d_b \gg d_a$, the PS volume, V_b, is given by

$$\begin{aligned} V_b &= f_b V \\ &\approx n \frac{\pi}{6} d_b^3 \end{aligned} \tag{A3}$$

where f_a and f_b are, respectively, the volume fraction of HDPE and PS calculated from the weight fraction and the density of each material employed. From Equations A2 and A3,

$$f_b \approx f_a \left(\frac{d_b}{d_a} \right)^3 \tag{A4}$$

or, alternatively

$$\begin{aligned} d_b &\approx d_a \left(\frac{f_b}{f_a} \right)^{1/3} \\ &\approx d_a \left(\frac{1 - f_a}{f_a} \right)^{1/3} \end{aligned} \tag{A5}$$

where d_b is the equivalent of L. Because T is given by

$$T = L - d_a \quad \text{(A6)}$$

Equation A5 can be written as

$$T \approx d_a \left[\left(\frac{1 - f_a}{f_a} \right)^{1/3} - 1 \right] \quad \text{(A7)}$$

References

1. P. BREADMORE and S. RABINOWITZ, *Appl. Polym. Symp.* **24** (1974) 25.
2. R. W. HERTZBERG, in "Deformation and Fracture Mechanics of Engineering Materials" (Wiley, New York, 1976) 605 pp.
3. B. BUCKNALL and W. W. STEVENS, *J. Mater. Sci.* **15** (1980) 2950.
4. J. A. SAUER and C. C. CHEN, *Adv. Polym. Sci.* **52/53** (1983) 169.
5. T. A. MORELLI and M. T. TAKEMORI, *J. Mater. Sci.* **18** (1983) 1836.
6. J. A. MANSON, R. W. HERTZBERG, M. J. CARLING, M. T. HAHN, J. HWANG, J. TURKANIS and G. ATTALLA, in "Toughening of Plastics II", (Plastics and Rubber Institute, London, 1985) p. 5.
7. J.-F. HWANG, J. A. MANSON, R. W. HERTZBERG, G. A. MILLER and L. H. SPERLING, *Polym. Eng. Sci.* **29** (1989) 1477.
8. J. A. SAUER and M. HARA, *Adv. Polym. Sci.* **91/92** (1990) 69.
9. E. J. MOSKALA, *J. Appl. Polym. Sci.* **49** (1993) 53.
10. M. G. WYZGOSKI and G. E. NOVAK, *ibid.* **51** (1994) 873.
11. H. R. AZIMI, R. A. PEARSON and R. W. HERTZBERG, *J. Mater. Sci. Lett.* **13** (1994) 1460.
12. S. R. SEIBEL, A. MOET, D. H. BANK and K. SEHANOBISH, *SPE ANTEC Tech. Papers* **41** (1995) 3966.
13. E. J. MOSKALA, *J. Mater. Sci.* **31** (1996) 507.
14. H. R. AZIMI, R. A. PEARSON and R. W. HERTZBERG, *J. Mater. Sci.* **31** (1996) 3777.
15. W. M. BARENTSEN and D. HEIKENS, *Polymer* **14** (1973) 579.
16. D. HEIKENS and W. M. BARENTSEN, *ibid.* **18** (1977) 69.
17. C. R. LINDSEY, J. W. BARLOW and D. R. PAUL, *J. Appl. Polym. Sci.* **26** (1981) 1.
18. R. FAYT, R. JÉRÔME and PH. TEYSSIÉ, *J. Polym. Sci. Polym. Lett. Ed.* **19** (1981) 79.
19. T. APPLEBY, F. CSER, G. MOAD, E. RIZZARDO and C. STAVROPOULOS, *Polym. Bull.* **32** (1994) 479.
20. M. BOUSMINA, P. BATAILLE, S. SAPIEHA and H. P. SCHREIBER, *Compos. Interfaces* **2** (1994) 171.
21. H. EL KADI, J. DENAULT, D. TAPIN, M. F. CHAMPAGNE, L. A. UTRACKI and M. M. DUMOULIN, *SPE ANTEC Tech. Papers* **41** (1995) 3143.
22. M. N. BUREAU, H. EL KADI, J. DENAULT, J. I. DICKSON and S. FRÉCHINET, *ibid.* **42** (1996) 2220.
23. M. N. BUREAU, H. EL KADI, J. DENAULT and J. I. DICKSON, *Polym. Eng. Sci.* **37** (1997) 377.
24. M. N. BUREAU, J. I. DICKSON and J. DENAULT, *J. Mater. Sci.*, in press.
25. J. P. ELINCK, J. C. BAUWENS and G. HONES, *Int. J. Fract. Mech.* **7** (1971) 277.
26. T. KUROBE and H. WAKASHIMA, *J. Soc. Mater. Sci.* **21** (1972) 800.
27. R. W. HERTZBERG and J. A. MANSON, *J. Mater. Sci.* **8** (1973) 1554.
28. R. W. HERTZBERG, J. A. MANSON and M. D. SKIBO, *Polym Eng. Sci.* **15** (1975) 252.
29. R. W. HERTZBERG, J. A. MANSON and S. L. KIM, *J. Mater. Sci.* **12** (1977) 531.
30. A. S. ARGON and J. G. HANNOOSH, *Philos. Mag.* **36** (1977) 1195.
31. R. W. HERTZBERG, M. D. SKIBO and J. A. MANSON, *ASTM STP* **675** (1979) 471.
32. R. W. HERTZBERG and J. A. MANSON (eds), "Fatigue of Engineering Plastics" (Academic Press, New York, 1980) 295 pp.
33. C. B. BUCKNALL and P. DUMPLETON, *Polym. Eng. Sci.* **25** (1985) 313.
34. *Idem., ibid.* **27** (1987) 110.
35. M. T. TAKEMORI, *Adv. Polym. Sci.* **91/92** (1990) 263.
36. C. KOSTER, V. ALTSTÄDT, H. H. KAUSCH and W. J. CANTWELL, *Polym. Bull.* **34** (1995) 243.
37. M. D. SKIBO, R. W. HERTZBERG, J. A. MANSON and S. L. KIM, *J. Mater. Sci.* **12** (1977) 531.
38. M. KITAGAWA, *Bull. J. Soc. Mech. Eng.* **18** (1975) 240.
39. P. E. BRETZ, in "Fatigue of Engineering Plastics", edited by R. W. Hertzberg and J. A. Manson (Academic Press, New York, 1980) p. 159.
40. J. R. WHITE and J. W. TEH, *Polymer* **20** (1979) 764.
41. M. D. SKIBO, R. W. HERTZBERG and J. A. MANSON, *J. Mater. Sci.* **11** (1976) 479.
42. N. E. WATERS, *ibid.* **1** (1966) 354.
43. H. F. BORDUAS, N. H. WATTS and D. J. BURNS, *Polym. Eng. Sci.* **7** (1967) 90.
44. L. E. CULVER and D. J. BURNS, *J. Strain Anal.* **3** (1968) 193.
45. S. ARAD, J. C. RADON and L. E. CULVER, *J. Mech. Eng. Sci.* **13** (1971) 75.
46. B. MUKHERJEE and D. J. BURNS, *Exp. Mech.* **11** (1971) 433.
47. P. G. FAULKNER and J. R. ATKINSON, *J. Appl. Polym. Sci.* **15** (1971) 209.
48. J. C. RADON, *ibid.* **17** (1973) 3515.
49. R. W. HERTZBERG, J. A. MANSON and M. D. SKIBO, *Polymer* **19** (1978) 359.
50. J. D. FERRY, in "Viscoelastic Properties of Polymers", 3rd Edn (Wiley, New York, 1980) 641 pp.
51. R. ATTERMO and G. ÖSTBERG, *Int. J. Fract. Mech.* **7** (1971) 122.
52. D. HEIKENS, N. HOEN, W. M. BARENTSEN, P. PIET and H. LADAN, *J. Polym. Sci. Polym. Symp. Mech. Prop. Morphol. Copolym. Modi. Polym. Blends* **62** (1978) 309.
53. R. FAYT, R. JÉRÔME and PH. TEYSSIÉ, *J. Polym. Sci. Polym. Phys. Ed.* **19** (1981) 1269.
54. M. MATOS, P. LOMELLINI and B. D. FAVIS, *SPE ANTEC Tech. Papers* **40** (1994) 1517.
55. M. C. SCHWARZ, J. W. BARLOW and R. D. PAUL, *J. Appl. Polym. Sci.* **35** (1988) 2053.
56. R. FAYT, R. JÉRÔME and PH. TEYSSIÉ, *J. Polym. Sci. B, Polym. Phys.* **27** (1989) 775.
57. H. WELANDER and M. RIGDAHL, *Polymer* **30** (1989) 207.
58. L. A. UTRACKI, "Polymer alloys and blends: Thermodynamics and rheology" (Hanser, Munich, 1989) 356 pp.
59. P. C. PARIS and F. ERDOGAN, *J. Basic Eng. Trans.: ASME Ser. D* **85** (1963) 528.
60. Y. M. MAI and J. G. WILLIAMS, *J. Mater. Sci.* **14** (1979) 1933.
61. H. EL KADI, unpublished results.
62. M. N. BUREAU, E. DI FRANCESCO, J. DEVAULT and J. I. DICKSON, published in the Proceedings of Polyblends '97 SPEC: International Symposium on Polymer Blends, Alloys and Filled Systems held October 9–10th 1997 at Industrial Materials Institute of the National Research Council, Canada (Brucherville, Quebec), pp. 641–671.
63. C. B. BUCKNALL, *Adv. Polym. Sci.* **27** (1978) 121.
64. A. S. ARGON, R. E. COHEN, O. S. GEBIZLIOGHI and G. E. SCHWIER, *ibid.* **52/53** (1983) 275.
65. S. WU, *Polymer* **26** (1985) 1855.
66. S. Y. HOBBS, *Polym. Eng. Sci.* **26** (1986) 74.
67. J. A. SAUER, J. TRENT and C. C. CHEN, *ibid.* **29** (1989) 69.
68. A. S. ARGON and R. E. COHEN, *Adv. Polym. Sci.* **91/92** (1990) 301.
69. G. DAGLI, A. S. ARGON and R. E. COHEN, *Polymer* **36** (1995) 2173.
70. M. MATSUO, T. T. WANG and T. K. KWEI, *J. Polym. Sci. A-2* **10** (1972) 1085.
71. N. J. MILLS and N. WALKER, *Polymer* **17** (1976) 335.
72. G. PITMAN and I. M. WARD, *J. Mater. Sci.* **15** (1980) 635.
73. W. DÖLL and L. KÖNCZÖL, *Adv. Polym. Sci.* **91/92** (1990) 137.
74. M. G. SCHINKER, L. KÖNCZÖL and W. DÖLL, *Colloid. Polym. Sci.* **262** (1984) 230.
75. D. S. DUGDALE, *J. Mech. Phys. Solids* **8** (1960) 100.

Received 13 August
and accepted 23 October 1997